

VCM: Vision Concept Modeling Based on Implicit Contrastive Learning with Vision-Language Instruction Fine-Tuning

A PREPRINT

Run Luo^{1,2} Renke Shan³ Longze Chen^{1,2} Ziqing Liu¹ Lu Wang³
Min Yang^{1,2} Xiaobo Xia^{3,4}

¹Shenzhen Institute of Advanced Technology, Chinese Academy of Sciences

²University of Chinese Academy of Sciences

³National University of Singapore

⁴MoE Key Laboratory of Brain-inspired Intelligent Perception and Cognition,
University of Science and Technology of China

{R.LUO@SIAT.AC.CN XIAOBXIA.UNI@GMAIL.COM}

ABSTRACT

Large Vision-Language Models (LVLMs) are pivotal for real-world AI tasks like embodied intelligence due to their strong vision-language reasoning abilities. However, current LVLMs process entire images at the token level, which is inefficient compared to humans who analyze information and generate content at the conceptual level, extracting relevant visual concepts with minimal effort. This inefficiency, stemming from the lack of a visual concept model, limits LVLMs’ usability in real-world applications. To address this, we propose VCM, an end-to-end self-supervised visual concept modeling framework. VCM leverages implicit contrastive learning across multiple sampled instances and vision-language fine-tuning to construct a visual concept model without requiring costly concept-level annotations. Our results show that VCM significantly reduces computational costs (e.g., 85% fewer FLOPs for LLaVA-1.5-7B) while maintaining strong performance across diverse image understanding tasks. Moreover, VCM enhances visual encoders’ capabilities in classic visual concept perception tasks. Extensive quantitative and qualitative experiments validate the effectiveness and efficiency of VCM.

1 Introduction

Large Vision-Language Models (LVLMs) [1, 2, 3, 4, 5, 6, 7] play a critical role in addressing a wide range of vision-language tasks and have become a cornerstone for enabling general artificial intelligence to interact with the real world, such as in embodied intelligence and autonomous driving. However, current LVLMs [1, 5] process entire images at the token level, which is inefficient compared to humans, who analyze information and generate content at the conceptual level, extracting relevant visual concepts with minimal effort. This inefficiency becomes particularly pronounced when dealing with higher-resolution images or longer video inputs, which humans can easily handle, but LVLMs struggle with it due to the rapidly increasing computational cost. This limitation, arising from the lack of a visual concept model, restricts the usability of LVLMs in real-world applications.

In this work, we formally define the concept of a **visual concept model** for the first time. A visual concept model dynamically determines the required visual concepts, including their quantity and spatial locations, based on given instructions. Notably, previous methods [8, 9, 10] have attempted to improve the efficiency of LVLMs by compressing image features using variable-length queries or pruning features through attention mechanisms. However, these approaches fail to provide semantically meaningful visual features grounded in the corresponding spatial locations of the image, making them unsuitable for vision-language tasks beyond visual question answering. As such, they cannot be categorized as visual concept models. Moreover, constructing a true visual concept model typically requires extensive fine-grained annotations, which are prohibitively expensive. How to train a visual concept model using large-scale and coarse-grained vision-language instruction data remains an unexplored challenge.

[†]Equal contribution.

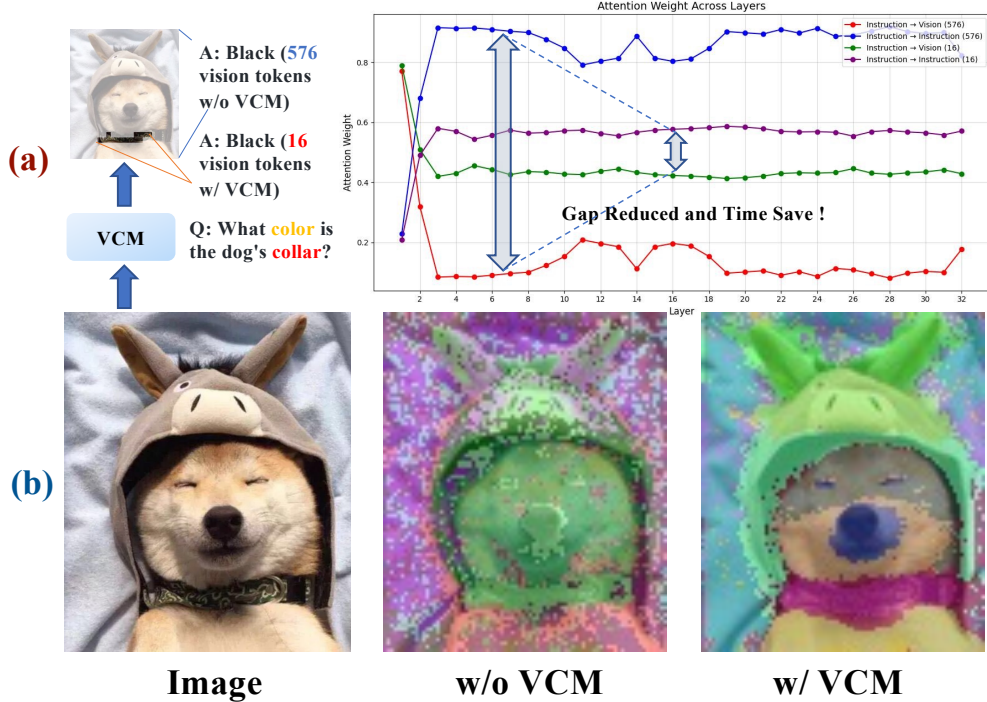


Figure 1: **Motivation of VCM.** VCM efficiently selects relevant visual concept tokens based on instructions, significantly reducing redundant attention computations in LVLMs. This reduction lowers both training and inference costs while maintaining strong performance, as shown in (a). Additionally, VCM enhances the dense concept prediction capability of the visual encoder, as illustrated in (b) through K-Means visualizations of dense feature maps from the last layer of CLIP ViT. These improvements enable broader applicability to vision-language tasks. The figure compares the results of the baseline model without VCM and the fine-tuned model incorporating VCM.

To address this, we propose VCM, an end-to-end self-supervised visual concept modeling framework. Specifically, VCM leverages implicit contrastive learning across multiple sampled instances and vision-language fine-tuning to construct a visual concept model without requiring costly concept-level annotations. To enable theoretical optimization for visual features of varying lengths, we design a forward-backward algorithm [11] that supports end-to-end dynamic length optimization. This allows the visual concept model to dynamically output the required visual concepts and their corresponding spatial locations according to the given instructions as shown in fig. 1. Benefiting from the visual concept model, VCM not only significantly reduces the computational cost of training and inference in LVLMs (e.g., 85% fewer FLOPs for LLaVA-1.5-7B) while maintaining strong visual question answering performance but also enhances the visual encoder’s capabilities in other vision-language tasks, such as zero-shot image classification, open-vocabulary object detection, and open-vocabulary semantic segmentation.

Before delving into details, our main contributions can be summarized as follows: (1) **Definition of the visual concept model.** We formally define the visual concept model, which dynamically determines the required visual concepts, including their quantity and spatial locations, based on given instructions. This model is applicable to a variety of vision-language tasks. (2) **The VCM framework.** We propose the VCM framework, which employs implicit contrastive learning across multiple sampled instances and a theoretically supported forward-backward algorithm to enable end-to-end dynamic visual concept learning without requiring expensive fine-grained annotations. (3) **Comprehensive experiments.** We conduct extensive qualitative analyses, quantitative experiments, and ablation studies to validate the effectiveness and efficiency of VCM.

2 Related Work

2.1 Large Vision-Language Models

Large Vision-Language Models (LVLMs) have rapidly advanced in recent years due to the success of Large Language Models (LLMs) and the availability of diverse image-text instruction data [1, 12, 13] from the internet. LLaVA [1] and

MiniGPT-4 [14] have demonstrated strong cross-task generalization by integrating visual encoders with large language models through simple connectors and training on instruction data. LLaVA-NeXT [2] has significantly enhanced visual perception by employing dynamic resolution techniques. DreamLLM [15] attempts to generate images and text in the interleaved context concurrently. DEEM [5] simplifies model architecture and enhances robustness by using diffusion models to extract visual features instead of traditional visual encoders. OpenOmni [16] further enhances the visual-language capabilities of the model by introducing the audio modality. The greater number and variety of inputs pose an even greater challenge for LVLMs.

2.2 Visual Token Reduction for LVLMs

Visual token reduction is a key technique for improving the efficiency of Large Vision-Language Models (LVLMs). Early works like EViT [17] and ToMe [18] reduce computational costs by pruning or compressing less important tokens, while methods such as LLaVolta [19], Qwen-VL [3], and MQT-LLaVA [20] use clustering or Q-former to compress tokens into fixed-length representations. Recent approaches like FastV [21], SparseVLM [9], PyramidDrop [22], and VisionZip [10] leverage language model signals and fixed pruning ratios to enhance efficiency, with LLaVA-Mini [23] further compressing entire images into a single visual token for tasks like visual question answering. However, these methods often disrupt implicit visual concept modeling due to over-compression, which introduces noise and misalignment between vision and concept that limit model applicability. To address this, we propose VCM, which uses rigorous theoretical optimization to enable dynamic visual token selection and end-to-end visual concept modeling first. VCM not only improves the efficiency of LVLMs but also broadens their applicability to diverse vision-language tasks.

3 Preliminaries

The LVLM architecture generally consists of three components: a visual encoder f_V , a modality projector f_M , and a large language model (LLM) f_{LLM} . The visual encoder, typically a pre-trained image encoder like CLIP’s vision model [24], converts input images \mathbf{X}^V into visual tokens $f_V(\mathbf{X}^V)$. The projector aligns these visual tokens with text instruction \mathbf{X}^I encoded by the LLM’s word embedding \mathbf{X}^T , which enables the LLM to process visual data effectively. For simplicity, we define that $\mathbf{H}^V = f_M(f_V(\mathbf{X}^V)) \in \mathbb{R}^{M \times d}$ and $\mathbf{H}^I = \mathbf{X}^I(\mathbf{X}^T)^\top \in \mathbb{R}^{N \times d}$, where M denotes the length of visual tokens, N denotes length of textual tokens, and d is the hidden dimension size. That is usually $M \gg N$. The LLM then integrates the aligned visual information and instructions to produce response \mathbf{X}^R , which is learned as $p_\theta(\mathbf{X}^R | f_{LLM}(\mathbf{H}^V, \mathbf{H}^I))$, parameterized by θ . Note that due to a large number of visual tokens, the training and inference of LVLMs are inefficient [21]. Therefore, if a visual concept model exists that can decrease the value of M , the efficiency of LVLMs during both training and inference will be largely improved. We provide more analysis of the efficiency improvement from the floating-point operations (FLOPs) perspective (see appendix D).

4 Vision Concept Modeling

The primary goal of visual concept modeling is to learn relevant visual conceptual information \mathbf{H}_C^V from $\mathbf{H}^{V\dagger}$, based on textual priors \mathbf{H}^I . The visual conceptual information can be applied to various vision-language tasks, leading to significant improvements in performance or efficiency. There are two key challenges in visual concept modeling. (1) Fine-grained labeled data is scarce, as manual annotation is labor-intensive, time-consuming, and inefficient. This makes it difficult to leverage the abundant unlabeled VQA datasets effectively. (2) The length of visual concepts varies dynamically across different examples, making it challenging to model and optimize. Below we present how to handle the two challenges and implement visual concept modeling.

4.1 Implicit Contrastive Learning

To address the challenge of limited fine-grained annotations, we propose an implicit contrastive learning approach based on randomly masking instruction keywords. The core idea, as illustrated in fig. 2, is that different instructions correspond to different regions of the image, which we define as the information domain. For instance, the instruction “Can you describe the image in detail?” requires information from the entire image, whereas “Where is the person in yellow?” only requires information from a specific region of the image. Moreover, even within the same instruction, different words carry varying amounts of information. For example, in the instruction “Where is the $< mask >$ in

[†] Here \mathbf{H}_C^V is a sparse version of \mathbf{H}^V , with $\|\mathbf{H}_C^V\|_0 \ll \|\mathbf{H}^V\|_0$.

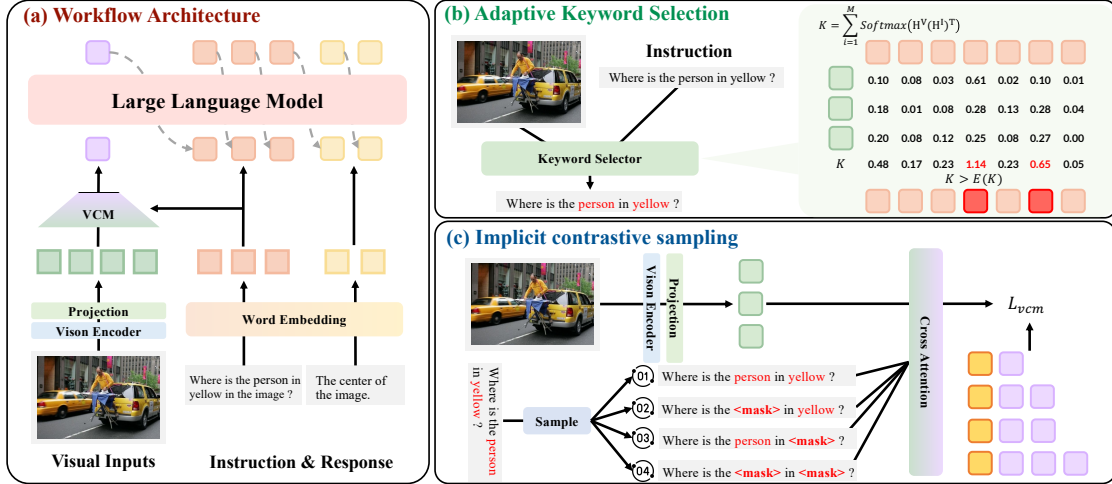


Figure 2: **Overview of our VCM framework.** (a) The workflow architecture: visual concepts are extracted from image inputs based on instruction priors and fed into the LLM to generate corresponding answers. (b) Adaptive keyword selection module: image-relevant keywords (highlighted in red) are selected by calculating text-image similarity, retaining keywords with scores above the average. (c) Implicit contrastive sampling module: keywords in the instruction are randomly masked, and the VCM loss is computed with input image features for end-to-end optimization.

yellow?”, the information amount is larger than “Where is the person in < mask >?”. Besides, removing non-keywords such as “is” or “in” has minimal impact on the information domain. Although it is hard to determine the exact size of the information domain for different instructions or words, we hypothesize that the number of keywords in an instruction is inversely proportional to the size of the corresponding information domain. The same instruction with different keyword mask ratios forms implicit contrastive learning samples.

To model this relationship, we randomly mask keywords in the instruction with a masking ratio $r \sim \text{Uniform}(0, 1)$ and estimate the corresponding visual token length. By training a model with this implicit contrastive learning process, we can capture the relationship between keywords and their corresponding visual regions without requiring explicit labels. The keywords are adaptively determined using the following formula:

$$K = \sum_{i=1}^M \text{Softmax}(\mathbf{H}^V(\mathbf{H}^I)^\top), \quad (1)$$

where an indicator function $\mathbb{I}_K(k > \mathbb{E}(K))$ is used to extract the keyword set from \mathbf{X}^I .

4.2 Visual Token Selection via Dynamic Programming

To tackle the challenge of dynamically varying visual concept lengths, we propose a forward-backward algorithm for dynamic visual token selection, enabling end-to-end optimization. For aligned visual tokens \mathbf{H}^V of length M , given textual priors \mathbf{H}^I with a masking ratio r , we use a binary classification head h to obtain classification results as follows:

$$\mathbf{Y}^V = h(\text{CrossAtt}(\mathbf{H}^V, \mathbf{H}^I)) = [\mathbf{y}_1^V, \dots, \mathbf{y}_M^V]. \quad (2)$$

The target visual token length is linearly estimated as $L = \lfloor M \cdot r \cdot S \rfloor$, where S is the information domain scalar. However, since we can only estimate the target length L without knowing the exact positions of these features, multiple alignment possibilities exist. Exhaustively searching all alignments has a time complexity of $\mathcal{O}(2^M)$, which is computationally prohibitive. To address this, we introduce mild assumptions to reformulate the problem into a dynamic programming process with a time complexity of $\mathcal{O}(M^2)$.

Assumption 1 (Context independence). All elements in \mathbf{Y}^V are context-independent.

This assumption is used to allow the total probability to be decomposed into the sum of individual state probabilities.

Assumption 2 (Information domain constraint). The information domain scalar S is constrained to $(0, 1/2]$.

This assumption is used to ensure successful state transitions during dynamic programming, the expanded target visual feature length $2L + 1$ must satisfy $2L + 1 \leq M$. Theoretically, this implies $S \leq 1/2$. Empirically, we observe that training vision-language models requires at most half of the visual features, as demonstrated by FastV [21], validating the reasonableness of this assumption.

Extension of target sequence. The target sequence \mathbf{Z}^V is initialized as a sequence of L symbols, where each symbol represents a retained visual token $\mathbf{Z}^V = \{\mathbf{z}_i^V\}_{i=1}^L$ with $\mathbf{z}_i^V \in \{\star\}$, where \star indicates a retained token. To account for possible alignments, the target sequence \mathbf{Z}^V is extended by inserting blank symbols \emptyset between and around the retained tokens $\mathbf{Z}^V = [\emptyset, \mathbf{z}_1^V, \emptyset, \mathbf{z}_2^V, \emptyset, \dots, \mathbf{z}_L^V, \emptyset]$. The length of the extended sequence \mathbf{Z}^V is hence $2L + 1$.

Forward probability initialization. The forward variable $\alpha(M, l)$ represents the probability of aligning the first t tokens of the input sequence to the first l tokens of the extended target sequence. The initialization is as follows. At the first time step $t = 1$, we set $\alpha(1, 1) = \mathbf{y}_1^V(\emptyset)$, where $\mathbf{y}_1^V(\emptyset)$ is the probability of aligning the first input token to the first blank symbol in the extended target sequence. For $l > 1$, the forward variable is initialized to $\alpha(1, l) = 0$ for $l > 1$.

Forward probability transition. The forward probabilities are computed iteratively from $t = 2$ to M and $l = 1$ to $2L + 1$ using the following recurrence relation: $\alpha(M, l) = \mathbf{y}_t^V(\mathbf{z}_l^V) \cdot (\alpha(t - 1, l) + \alpha(t - 1, l - 1))$, where $\mathbf{y}_t^V(\mathbf{z}_l^V)$ is the probability of aligning the t -th input token to the l -th token in the extended target sequence, $\alpha(t - 1, l)$ represents the probability of staying at the current state, and $\alpha(t - 1, l - 1)$ represents the probability of transitioning from the previous state.

Backward probability initialization. The backward variable $\beta(M, l)$ represents the probability of aligning the remaining tokens of the input sequence (from $t + 1$ to M) to the remaining tokens of the extended target sequence (from $l + 1$ to $2L + 1$). The initialization is as follows. At the last time step ($t = M$), $\beta(M, 2L + 1) = 1$, where $2L + 1$ is the final blank symbol in the extended target sequence. For $l < 2L + 1$, the backward variable is initialized to $\beta(M, l) = 0$ for $l < 2L + 1$.

Backward probability transition. The backward probabilities are computed iteratively from $t = M - 1$ to 1 and $l = 2L$ to 1 using the following recurrence relation: $\beta(M, l) = \beta(t + 1, l) \cdot \mathbf{y}_{t+1}^V(\mathbf{z}_l^V) + \beta(t + 1, l + 1) \cdot \mathbf{y}_{t+1}^V(\mathbf{z}_l^V)$, where $\beta(t + 1, l)$ represents the probability of staying at the current state, and $\beta(t + 1, l + 1)$ represents the probability of transitioning to the next state.

4.3 Objective of VCM and Gradient Computation

The total probability of the extended target sequence \mathbf{Z}^V given the input sequence \mathbf{Y}^V is computed as:

$$p(\mathbf{Z}^V | \mathbf{Y}^V) = \sum_{l=1}^{2L+1} \alpha(M, l) \cdot \beta(M, l). \quad (3)$$

The loss is then defined as the negative log-likelihood:

$$\mathcal{L}_{\text{VCM}} = -\log p(\mathbf{Z}^V | \mathbf{Y}^V). \quad (4)$$

The gradient of the loss with respect to $\mathbf{y}_t^V(\mathbf{z}_l^V)$ is computed using the posterior probability $\gamma(t, l)$, which represents the probability of aligning the t -th input token to the l -th token in the extended target sequence:

$$\gamma(t, l) = \frac{\alpha(M, l) \cdot \beta(M, l)}{p(\mathbf{Z}^V | \mathbf{Y}^V)}. \quad (5)$$

The gradient is then given by: $\frac{\partial \mathcal{L}_{\text{VCM}}}{\partial \mathbf{y}_t^V(\mathbf{z}_l^V)} = \mathbf{y}_t^V(\mathbf{z}_l^V) - \gamma(t, l)$ (see appendix C), where an indicator function $\mathbb{I}_{\mathbf{Y}^V}(p(\star | \mathbf{y}_t^V) > P(\emptyset | \mathbf{y}_t^V))$ is used to extract the visual concept \mathbf{H}_C^V from \mathbf{H}^V via segment merging (SM) operation $\mathbf{H}_C^V = \text{SM}(\mathbf{H}^V, \mathbf{Y}^V, \mathbb{I}_{\mathbf{Y}^V}(p(\star | \mathbf{y}_t^V) > P(\emptyset | \mathbf{y}_t^V)))$, as shown in fig. 3. Besides, for better understanding, we provide detailed pseudo codes for the SM operation in appendix E (100x faster than a double loop). The weighted average method is used to extract the concept level features \mathbf{H}_C^V from the features \mathbf{H}^V of the token level, giving the physical meaning of the importance of the score \mathbf{Y}^V , which is more suitable for other scenarios. The next prediction loss is defined as:

$$\mathcal{L}_{\text{NTP}} = -\log p(\mathbf{X}^R | h_{\text{LLM}}(\mathbf{H}_C^V, \mathbf{H}^I)).$$

The total loss is then defined as:

$$\mathcal{L}_{\text{total}} = \mathcal{L}_{\text{NTP}} + \epsilon(r) \cdot \mathcal{L}_{\text{VCM}},$$

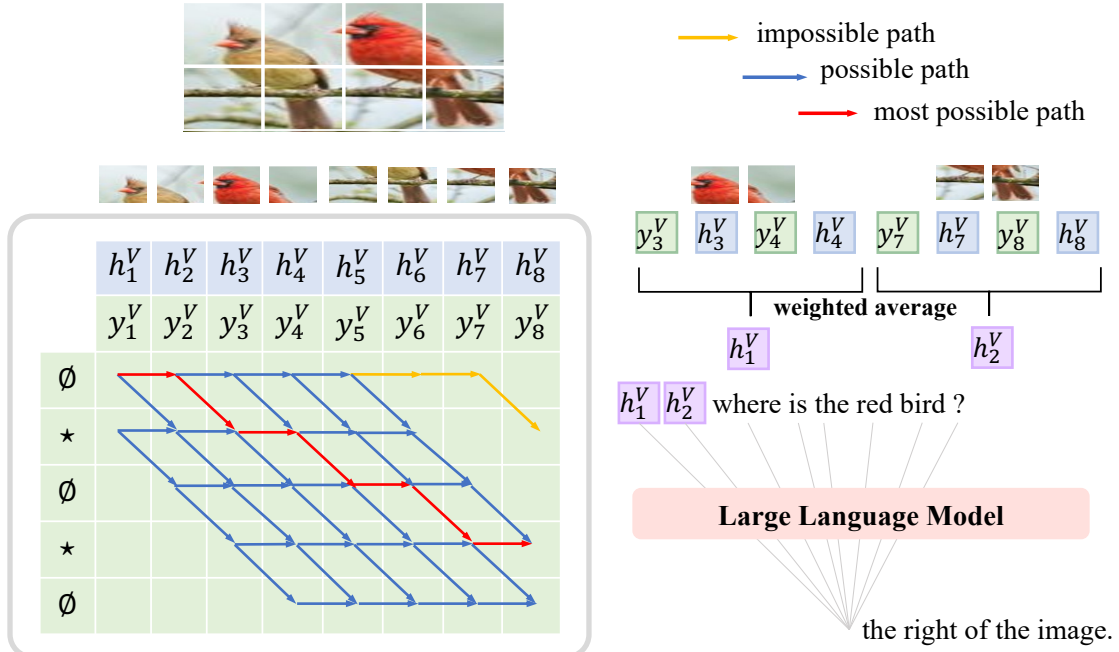


Figure 3: **An example of the workflow in VCM.** The VCM loss computes all possible alignment paths with the extended target sequence, maximizing the probabilities of feasible paths (blue paths) while minimizing the probabilities of infeasible paths (yellow paths), ensuring that the output concept length meets expectations. During training and inference, the most probable path (red path) is selected, and a segment merging operation (SM) is performed, where adjacent retained visual features are weighted and averaged based on their probability scores. The extracted visual concept features are then combined with the instruction and fed into the LLM to generate the corresponding answer in an end-to-end manner.

where $\epsilon(r)$ is a coefficient function used to balance two loss functions. When the mask ratio r is small, the VCM loss is not so accurate, the coefficient is appropriately small. Besides, when r is large, the VCM loss is more accurate and appropriately increases, using the hyperbolic tangent smoothing function. More details can be found in appendix B.

5 Experiments

Datasets. To justify our claims and demonstrate the superiority of VCM, several representative tasks are involved here, which include visual question answering, open-vocabulary object detection, zero-shot image classification, and open-vocabulary semantic segmentation. Specifically, for visual question answering evaluation, we conduct experiments on 9 widely adopted benchmarks, including GQA [25], MMBench (MMB) [26], MME [27], POPE [28], SciQA [29], VQAV2 [30] (VQA V2), SEED-Image (SEED) [31] and MMvet [32]. LMMs-Eval toolkit [33] is used for fair comparison. Besides, we employ the COCO [34] dataset for open-vocabulary object detection and zero-shot image classification. Besides, for open-vocabulary semantic segmentation, ADE250 [35] and ADE847 [35] are utilized. More details of the tasks and datasets are included in appendix E.

Models. We follow the architecture from LLaVA series [1, 2], where a multimodal large model consists of three key components: an LLM for next token prediction, a visual encoder for extracting visual features, and an image-text projector to align the visual and text modalities. One layer of transformer is used for applying the cross-attention operation in VCM. For LLaVA-1.5-7/13B and LLaVA-NeXT [2], we use the same inference setting as the original paper because it is publicly available.

Training strategies. We follow the widely used two-stage setting to conduct the training of VCM. Specifically, it includes vision-language pre-training and vision-language instruction-tuning. The language models and ViT are separately pre-trained, while the projector is randomly initialized. To initially align the feature space between the visual

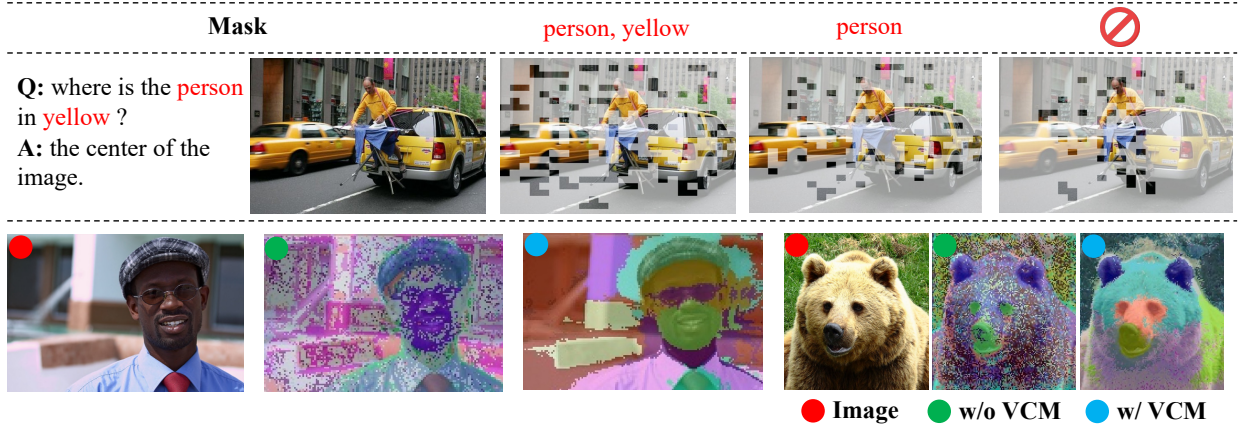


Figure 4: **Visualization of VCM.** (a) Visualization of VCM on different instructions. From left to right, the visual representation becomes increasingly sparse, leaving corresponding vision tokens to unmasked keywords (highlighted in red). (b) K-Means visualization of dense feature maps of CLIP ViT. We show the raw images, the K-Means results without VCM, and those of our fine-tuned model by VCM.

Table 1: Performance on 9 image-based benchmarks. ‘Res.’ is resolution, and ‘#Vision Tokens’ is the number of vision tokens fed to the LLM backbone. ‘*’ indicates that unfreezing the image encoder in the instruction fine-tuning stage.

Methods	LLM	Res.	#Vision Tokens	VQA ^{v2}	GQA	VisWiz	SciQA	POPE	MME	MMB	SEED	MM-Vet	Avg. (%)
BLIP-2 [36]	Vicuna-13B	224	32	65.0	41.0	19.6	61.0	85.3	1293.8	–	46.4	22.4	–
InstructBLIP [4]	Vicuna-7B	224	32	–	49.2	34.5	60.5	–	–	36.0	53.4	26.2	–
IDEFICS-9B [37]	LLaMA-7B	224	64	50.9	38.4	35.5	–	–	–	48.2	–	–	–
IDEFICS-80B [37]	LLaMA-65B	224	64	60.0	45.2	36.0	–	–	–	54.5	–	–	–
Qwen-VL [3]	Qwen-7B	448	256	78.8	59.3	35.2	67.1	–	–	38.2	56.3	–	–
Qwen-VL-Chat [3]	Qwen-7B	448	256	78.2	57.5	38.9	68.2	–	1487.5	60.6	58.2	–	–
SPHINX [38]	LLaMA-13B	224	289	78.1	62.6	39.9	69.3	80.7	1476.1	66.9	56.2	36.0	–
mPLUG-Owl2 [39]	LLaMA-7B	448	1024	79.4	56.1	54.5	68.7	–	1450.2	64.5	57.8	36.2	–
LLaVA-v1.5 [1]	Vicuna-7B	336	576	78.5	62.0	50.0	66.8	85.9	1510.7	64.3	58.6	30.5	63.6
LLaVA-v1.5* [1]	Vicuna-7B	336	576	77.6	61.7	46.5	66.5	86.0	1423.3	64.1	57.3	30.2	62.3
<i>LMMs with fewer vision tokens</i>													
MQT-LLaVA [8]	Vicuna-7B	336	36	73.7	58.8	51.0	66.8	81.9	1416.3	63.4	–	27.8	–
PruMerge [40]	Vicuna-7B	336	32	72.0	–	–	68.5	76.3	1350.3	60.9	–	–	–
PruMerge++ [40]	Vicuna-7B	336	144	76.8	–	–	68.3	84.0	1462.4	64.9	–	–	–
FastV [21]	Vicuna-7B	336	64	55.0	46.1	–	51.1	48.0	987.1	48.0	51.9	25.8	46.9
SparseVLM [9]	Vicuna-7B	336	64	68.2	52.7	–	62.2	75.1	1272.5	56.2	51.1	23.3	55.9
VisionZip [10]	Vicuna-7B	336	64	72.4	55.1	50.1	69.0	77.0	1342.1	60.1	52.2	31.7	59.4
VisionZip† [10]	Vicuna-7B	336	64	74.2	57.0	50.5	68.8	80.9	1369.4	61.5	53.4	30.2	60.1
<i>Ours</i>													
VCM	Vicuna-7B	336	64	74.6	57.8	56.2	69.4	85.3	1440.7	62.3	56.3	29.8	62.7
Δ compare to LLaVA-v1.5				-3.9	-4.2	+6.2	+2.6	-0.6	-70.0	-2.0	-2.3	-0.7	-0.9
VCM*	Vicuna-7B	336	64	73.2	56.9	54.8	68.3	84.7	1410.5	62.7	55.9	29.5	61.9
Δ compare to LLaVA-v1.5*				-4.4	-4.8	+8.3	+1.8	-1.3	-12.8	-1.4	-1.4	-0.7	-0.4

and text modalities, we utilize an aligned dataset [1]. Afterward, we perform instruction tuning of the pre-trained model on visual language instruction datasets. The AdamW optimizer [41] is exploited, with learning rates 5×10^{-5} and 2×10^{-5} for aforementioned two stages respectively. The instruction fine-tuning stage is trained with two epochs with a 3% warmup strategy. The experiments are conducted with $8 \times$ NVIDIA A100-80G GPUs.

5.1 Qualitative Analysis

As shown in fig. 4(a), we visualize the performance of VCM on visual question-answering (VQA) examples. From left to right, we demonstrate the results of masking different numbers of keywords in the instruction. As fewer keywords (highlighted in red) are masked, more irrelevant tokens are removed, and the visual concepts are progressively refined.

Table 2: High resolution performance on 6 image-based benchmarks. The best result in each case is shown in bold.

Methods	#Vision Tokens	VQA ^{v2}	GQA	SciQA	POPE	MME	MMB	Avg. (%)
LLaVA-v1.6	2880	80.1	64.2	70.2	86.5	1842.1	67.9	72.4
SparseVLM	160	66.3	51.2	67.5	74.8	1542.1	63.1	63.0
VisionZip	160	71.4	55.5	68.3	83.4	1630.2	60.1	66.2
VisionZip [‡]	160	75.6	58.2	67.5	85.7	1699.0	63.9	68.6
VCM	160	76.8	60.1	69.6	87.1	1723.4	65.5	70.1

Table 3: Experiment of zero-shot image classification on COCO. The best result in each case is shown in bold.

CLIP	VCM	Thing Masks		Stuff Masks	
		Top 1	Top 5	Top 1	Top 5
ViT-B/16	×	33.5	56.0	25.9	50.9
ViT-B/16	✓	42.7	70.6	39.8	64.6
ViT-L/14	×	28.3	52.0	11.8	27.9
ViT-L/14	✓	43.8	69.7	25.4	47.0

The visualizations indicate that, although VCM discards some overall image details, it effectively retains the key visual concepts required for correctly answering the question. Additional visualization cases can be found in appendix F.

We further demonstrate the visual concept representation of the visual encoder trained with VCM by performing K-Means clustering [42] on the dense feature maps. Specifically, pixels with high cosine similarity are grouped into the same cluster. For clarity, clusters containing only a small number of pixels are removed. As shown in fig. 4(b), the CLIP ViT trained with VCM exhibits significantly improved performance in grouping pixels belonging to the same object into a single cluster, compared to the baseline without VCM. For example, in the visualization, clusters corresponding to “face”, “hat”, and “glasses” are notably more accurate. These K-Means clustering results provide intuitive evidence for the enhanced visual concept representation capability of CLIP ViT. More visualization cases can be found in appendix F.

5.2 Benchmark Comparison

To evaluate the effectiveness of our method on visual question answering, we conduct experiments on 9 widely used benchmarks and compare our method against existing state-of-the-art (SOTA) methods. These methods [21, 9, 10, 8] typically reduce the number of visual tokens in the LLM forward process using attention weights or a small number of queries. Additionally, to further validate the generalizability of our method, we conduct experiments on high-resolution scenarios. Beyond VQA, we also evaluate the visual concept learned by the VCM-trained CLIP ViT on other vision-language tasks, including zero-shot image classification, open-vocabulary object detection, and open-vocabulary semantic segmentation. More visualization case can be found in appendix F.

Results on VQA. As shown in section 5, we apply VCM to train LLaVA-1.5 and evaluate its performance on VQA tasks. When retaining only 64 tokens, our method outperforms FastV [21], SparseVLM [9], and VisionZip[‡] [10] by 33.7%, 12.3%, and 4%, respectively. Furthermore, compared to the original LLaVA-1.5, VCM achieves 98.6% of the performance of the vanilla model, even with only 64 visual tokens retained. This represents only a 1.4% drop in accuracy compared to the baseline using 10 times more visual tokens. If the visual encoder is unfrozen during training, this gap can be reduced to 0.6%, justifying the VCM’s superiority.

Results on VQA for high-resolution scenarios. To further demonstrate the generalization capabilities of VCM, we apply it to LLaVA-NeXT [2], which supports high-resolution scenarios. Compared to LLaVA-1.5, LLaVA-NeXT divides the image into four parts, resizes the original image, and converts it into five independent images. The visual encoder processes each image to extract visual tokens, which are then merged. While this method improves model performance, it significantly increases the number of visual tokens. As shown in table 2, our proposed VCM consistently maintains strong performance under high-resolution settings. Specifically, when reducing the number of visual tokens to only 5% of the original one, our method achieves 96.8% performance, outperforming SparseVLM and VisionZip[‡] by 11.3% and 2%, respectively. Furthermore, VCM demonstrates outstanding performance on visual hallucination tasks (e.g., POPE), validating its effectiveness in concept extraction and sample selection for high-resolution images.

Table 4: Experiment of open-vocabulary object detection on COCO. The best result in each case is shown in bold.

Method	CLIP	OV-COCO		
		AP_{50}^{novel}	AP_{50}^{base}	AP_{50}
F-VLM	ViT-B/16	16.0	36.9	31.4
F-VLM+VCM	ViT-B/16	20.6	47.1	38.6
F-VLM	ViT-L/14	9.2	44.3	35.2
F-VLM+VCM	ViT-L/14	12.6	48.7	39.2

Table 5: Experiments of open-vocabulary semantic segmentation on COCO. The best result in each case is shown in bold.

Method	CLIP	ADE-150		ADE-847	
		mIoU	mAcc	mIoU	mAcc
SAN [47]	ViT-B/16	27.5	45.6	10.1	21.1
SAN [47]	ViT-L/14	32.1	50.7	12.4	25.2
Cat-Seg [48]	ViT-B/16	27.2	41.2	8.4	16.6
Cat-Seg [48]	ViT-L/14	31.5	46.2	10.8	20.5
Cat-Seg+VCM	ViT-B/16	29.4	45.5	9.1	21.3
Cat-Seg+VCM	ViT-L/14	34.8	53.1	11.9	23.1

Results on zero-shot image classification. We also evaluate the visual concept perception capabilities of the VCM-trained CLIP ViT on zero-shot image classification on the COCO validation set [34]. Specifically, we extract dense feature maps from the CLIP ViT using panoptic masks (thing and stuff) from the COCO Panoptic dataset [43] and mask pooling operations [44]. The corresponding mean accuracy (mAcc) is reported in table 3. The results show that VCM significantly improves the classification capabilities of CLIP ViT on panoptic masks, establishing VCM as a promising solution for enhancing the visual concept representation capabilities of visual encoders.

Results on open-vocabulary object detection. Following the setup of F-VLM [45], we freeze the CLIP backbone and introduce a two-stage detector baseline. To extract multi-scale feature maps from the frozen backbone, we interpolate the feature maps from intermediate layers of the ViT. As shown in table 4, replacing the CLIP ViT with the VCM-trained version significantly improves performance on OV-COCO [46] (e.g., 9.2 vs. 12.6 for AP_{50}^{novel} , 44.3 vs. 48.7 for AP_{50}^{base} , and 35.2 vs. 39.2 for AP_{50}). These results highlight the effectiveness of VCM in open-vocabulary object detection.

Results on open-vocabulary semantic segmentation. We apply the VCM fine-tuned model to CatSeg [49], where the dense features of CLIP ViT are utilized in a cost-aggregation module. The segmentation model is trained on the COCO Stuff dataset [48] and evaluated on the ADE20K dataset [35], including ADE-150 and ADE-847. As shown in table 5, VCM consistently improves performance across all test datasets.

5.3 Ablation Study

To investigate the impact of model design, information domain selection, and scalability on performance, we conduct comprehensive ablation studies under the default configuration. All experiments are performed using 8×NVIDIA A100-80G GPUs. The batch size is set to 64. The number of training steps is set to 500.

Ablation study on model component design. We conduct ablation experiments on the coefficient function and the weighted averaging operation, both using the same default configuration. As shown in table 6, employing the tanh smoothing function as the coefficient function significantly enhances overall model performance, particularly in its ability to mitigate hallucination, which validates the effectiveness of the coefficient function design. Furthermore, incorporating a weighted averaging method in the concept extraction process, which integrates importance scores into the end-to-end next-token prediction optimization, further improves the overall model performance and accelerates model convergence.

Ablation study on information domain S . We also perform ablation studies on the choice of the information domain under the default configuration. As shown in table 7, a larger information domain, which retains more visual information, generally leads to better performance. However, as the information domain size decreases, the shorter sampling length

Table 6: Ablation Study of the coefficient function $\epsilon(r)$ and weighted average method in SM on four VQA benchmarks. The best result in each case is shown in bold.

$\epsilon(r)$	weighted average	SciQA	VizWiz	POPE	MME	Avg.
×	×	60.7	46.5	73.4	931.5	56.8
✓	×	61.7	46.7	75.4	935.2	57.6
✓	✓	64.1	48.2	76.6	950.6	59.1

Table 7: Ablation Study of information domain S on four VQA benchmarks. The best result in each case is shown in bold.

S	#Max Tokens	SciQA	VizWiz	POPE	MME	Avg.
1/2	288	62.9	46.9	76.8	1039.7	59.7
1/4	144	64.1	48.2	76.6	950.6	59.1
1/6	72	61.1	46.4	74.0	934.9	57.1
1/8	36	61.7	46.6	76.1	944.1	58.0

Table 8: Ablation study of VCM scalability on four VQA benchmarks. The best result in each case is shown in bold.

LLM	Data	SciQA	VizWiz	VQA ^{v2}	GQA	Avg.
Vicuna-7b	556K	64.1	48.2	56.8	43.6	53.2
Vicuna-7b	790K	65.4	49.7	59.3	46.1	55.1
Vicuna-13b	790K	67.8	53.1	62.3	49.5	58.2

stabilizes training and can result in additional performance gains. Specifically, selecting an information domain size of 1/4 achieves a favorable trade-off between computational cost and performance, as it maintains competitive accuracy while significantly reducing FLOPs. Based on these findings, we adopt the 1/4 information domain configuration across all experiments.

Ablation study on scalability. To explore whether VCM can achieve further performance gains through increased data and model scale, we conduct experiments using a larger dataset used in LLaVA-NeXT [2] and a larger language model (Vicuna-13B) under the default configuration. As shown in table 8, increasing the amount of instruction-tuning data and scaling up the language model both consistently improve performance, which demonstrates the strong scalability of our VCM.

6 Conclusion

In this paper, we propose a visual concept model that efficiently extracts visual concept for various vision-language tasks. VCM utilizes large-scale vision-language instruction data with coarse labels, employs implicit contrastive sampling, and integrates a dynamic concept extraction algorithm optimized through a forward-backward framework for end-to-end training. Extensive experiments demonstrate that our method reduces computational costs while maintaining strong performance on VQA benchmarks and enhances the visual encoder’s conceptual understanding in tasks like zero-shot classification, open-vocabulary detection, and segmentation. Ablation studies further validate its effectiveness and scalability.

7 Impact Statement

The deployment and release of VCM present both potential advantages and risks. These considerations include visual-related factors as well as common challenges observed in existing LLMs, such as Alpaca and Vicuna. Since VCM is built on LLaMA, Vicuna, and CLIP, it inherits certain limitations associated with LLMs and vision encoders. Below, we highlight the key risks and the mitigation strategies designed for the release of this model.

Hallucination. Like other LLMs, VCM may generate outputs that are not grounded in factual information or input data. This raises concerns about the reliability of its inferences, particularly in high-stakes applications such as the medical domain.

Biases. VCM may inherit biases from its base models, including the vision encoder (CLIP) and the language decoder (LLaMA/Vicuna). These biases could lead to skewed outcomes or unfair representations of diverse content.

A Limitation

In our experiments, we primarily rely on an adaptive keyword selection strategy. However, this approach introduces certain biases, as the selected keywords may not always represent true keywords. Additionally, to simplify modeling, we use the same information domain for different types of instruction data. This coarse-grained design may negatively impact the model’s performance. In the future, we aim to employ open-source language models to perform more refined information domain classification and keyword selection for instruction data. By providing finer-grained additional information, we hope to further improve the performance of our proposed method.

B Mathematical Expression of $\epsilon(r)$

The coefficient function $\epsilon(r)$ can be expressed mathematically as follows:

Step 1: Compute a smooth S-shaped function using the hyperbolic tangent (\tanh) function:

$$s = \frac{1 + \tanh(k \cdot (2 \cdot r - 1))}{2}, \quad (6)$$

where k is a parameter that controls the growth rate. Larger values of k result in steeper transitions, while smaller values result in smoother transitions.

Step 2: Scale and shift s to the desired range $[a, b]$:

$$\epsilon(r) = a + (b - a) \cdot s, \quad (7)$$

where $a = 0.2, b = 1.2, k = 5$ in our default setting.

C Proof of Gradient Computation $\frac{\partial \mathcal{L}_{\text{VCM}}}{\partial \mathbf{y}_t^{\text{V}}(\mathbf{z}_l^{\text{V}})}$

The VCM loss is defined as:

$$\mathcal{L}_{\text{VCM}} = -\log p(\mathbf{Z}^{\text{V}} | \mathbf{Y}^{\text{V}}), \quad (8)$$

where $p(\mathbf{Z}^{\text{V}} | \mathbf{Y}^{\text{V}})$ is the probability of the extended target sequence \mathbf{Z}^{V} conditioned on the input probability sequence \mathbf{Y}^{V} . It is computed as:

$$p(\mathbf{Z}^{\text{V}} | \mathbf{Y}^{\text{V}}) = \sum_{l=1}^{2L+1} \alpha(M, l) \cdot \beta(M, l), \quad (9)$$

where $\alpha(M, l)$ and $\beta(M, l)$ are the forward and backward variables, respectively. We aim to compute the gradient of the loss with respect to $\mathbf{y}_t^{\text{V}}(\mathbf{z}_l^{\text{V}})$, i.e., $\frac{\partial \mathcal{L}_{\text{VCM}}}{\partial \mathbf{y}_t^{\text{V}}(\mathbf{z}_l^{\text{V}})}$.

Step 1: Apply the Chain Rule

Using the chain rule, the gradient of \mathcal{L}_{VCM} with respect to $\mathbf{y}_t^{\text{V}}(\mathbf{z}_l^{\text{V}})$ is given by:

$$\frac{\partial \mathcal{L}_{\text{VCM}}}{\partial \mathbf{y}_t^{\text{V}}(\mathbf{z}_l^{\text{V}})} = -\frac{1}{p(\mathbf{Z}^{\text{V}} | \mathbf{Y}^{\text{V}})} \cdot \frac{\partial p(\mathbf{Z}^{\text{V}} | \mathbf{Y}^{\text{V}})}{\partial \mathbf{y}_t^{\text{V}}(\mathbf{z}_l^{\text{V}})}. \quad (10)$$

Therefore, the key is to compute $\frac{\partial p(\mathbf{Z}^{\text{V}} | \mathbf{Y}^{\text{V}})}{\partial \mathbf{y}_t^{\text{V}}(\mathbf{z}_l^{\text{V}})}$.

Step 2: Compute $\frac{\partial p(\mathbf{Z}^V | \mathbf{Y}^V)}{\partial \mathbf{y}_t^V(\mathbf{z}_l^V)}$

From the definition of $p(\mathbf{Z}^V | \mathbf{Y}^V)$, we have:

$$p(\mathbf{Z}^V | \mathbf{Y}^V) = \sum_{l=1}^{2L+1} \alpha(M, l) \cdot \beta(M, l). \quad (11)$$

Taking the derivative with respect to $\mathbf{y}_t^V(\mathbf{z}_l^V)$, we get:

$$\frac{\partial p(\mathbf{Z}^V | \mathbf{Y}^V)}{\partial \mathbf{y}_t^V(\mathbf{z}_l^V)} = \sum_{l=1}^{2L+1} \left(\frac{\partial \alpha(M, l)}{\partial \mathbf{y}_t^V(\mathbf{z}_l^V)} \cdot \beta(M, l) + \alpha(M, l) \cdot \frac{\partial \beta(M, l)}{\partial \mathbf{y}_t^V(\mathbf{z}_l^V)} \right). \quad (12)$$

Now, we need to compute $\frac{\partial \alpha(M, l)}{\partial \mathbf{y}_t^V(\mathbf{z}_l^V)}$ and $\frac{\partial \beta(M, l)}{\partial \mathbf{y}_t^V(\mathbf{z}_l^V)}$.

Step 3: Compute $\frac{\partial \alpha(M, l)}{\partial \mathbf{y}_t^V(\mathbf{z}_l^V)}$

The forward variable $\alpha(M, l)$ is defined recursively as:

$$\alpha(M, l) = \mathbf{y}_t^V(\mathbf{z}_l^V) \cdot (\alpha(t-1, l) + \alpha(t-1, l-1)). \quad (13)$$

Taking the derivative with respect to $\mathbf{y}_t^V(\mathbf{z}_l^V)$, we get:

$$\frac{\partial \alpha(M, l)}{\partial \mathbf{y}_t^V(\mathbf{z}_l^V)} = \begin{cases} \alpha(t-1, l) + \alpha(t-1, l-1), & \text{if } t = M, \\ 0, & \text{if } t \neq t. \end{cases} \quad (14)$$

For all $t' \neq t$, we have $\frac{\partial \alpha(t', l)}{\partial \mathbf{y}_t^V(\mathbf{z}_l^V)} = 0$ because $\alpha(t', l)$ is independent of $\mathbf{y}_t^V(\mathbf{z}_l^V)$.

Step 4: Compute $\frac{\partial \beta(M, l)}{\partial \mathbf{y}_t^V(\mathbf{z}_l^V)}$

The backward variable $\beta(M, l)$ is defined recursively as:

$$\beta(M, l) = \beta(t+1, l) \cdot \mathbf{y}_{t+1}^V(\mathbf{z}_l^V) + \beta(t+1, l+1) \cdot \mathbf{y}_{t+1}^V(\mathbf{z}_{l+1}^V). \quad (15)$$

For $t < M$, $\beta(M, l)$ does not directly depend on $\mathbf{y}_t^V(\mathbf{z}_l^V)$, so:

$$\frac{\partial \beta(M, l)}{\partial \mathbf{y}_t^V(\mathbf{z}_l^V)} = 0 \quad \text{for } t < M. \quad (16)$$

At $t = M$, $\beta(M, l)$ is initialized as 1 for $l = 2L + 1$ and 0 otherwise, and thus:

$$\frac{\partial \beta(M, l)}{\partial \mathbf{y}_t^V(\mathbf{z}_l^V)} = 0. \quad (17)$$

Step 5: Simplify $\frac{\partial p(\mathbf{Z}^V | \mathbf{Y}^V)}{\partial \mathbf{y}_t^V(\mathbf{z}_l^V)}$

Substituting the results for $\frac{\partial \alpha(M, l)}{\partial \mathbf{y}_t^V(\mathbf{z}_l^V)}$ and $\frac{\partial \beta(M, l)}{\partial \mathbf{y}_t^V(\mathbf{z}_l^V)}$, we simplify:

$$\frac{\partial p(\mathbf{Z}^V | \mathbf{Y}^V)}{\partial \mathbf{y}_t^V(\mathbf{z}_l^V)} = \sum_{l=1}^{2L+1} \frac{\partial \alpha(M, l)}{\partial \mathbf{y}_t^V(\mathbf{z}_l^V)} \cdot \beta(M, l). \quad (18)$$

Using $\frac{\partial \alpha(M, l)}{\partial \mathbf{y}_t^V(\mathbf{z}_l^V)} = \alpha(t-1, l) + \alpha(t-1, l-1)$, we have:

$$\frac{\partial p(\mathbf{Z}^V | \mathbf{Y}^V)}{\partial \mathbf{y}_t^V(\mathbf{z}_l^V)} = \sum_{l=1}^{2L+1} \beta(M, l) \cdot (\alpha(t-1, l) + \alpha(t-1, l-1)). \quad (19)$$

Step 6: Define Posterior Probability $\gamma(t, l)$

We define the posterior probability $\gamma(t, l)$ as:

$$\gamma(t, l) = \frac{\alpha(M, l) \cdot \beta(M, l)}{p(\mathbf{Z}^V | \mathbf{Y}^V)}. \quad (20)$$

This represents the probability of aligning the t -th token of \mathbf{y} to the l -th token of \mathbf{z} , given the entire alignment. Using this definition, we express the gradient as:

$$\frac{\partial \mathcal{L}_{\text{VCM}}}{\partial \mathbf{y}_t^V(\mathbf{z}_l^V)} = \mathbf{y}_t^V(\mathbf{z}_l^V) - \gamma(t, l). \quad (21)$$

Final Result

The gradient of the VCM loss with respect to $\mathbf{y}_t^V(\mathbf{z}_l^V)$ is:

$$\frac{\partial \mathcal{L}_{\text{VCM}}}{\partial \mathbf{y}_t^V(\mathbf{z}_l^V)} = \mathbf{y}_t^V(\mathbf{z}_l^V) - \gamma(t, l), \quad (22)$$

where $\gamma(t, l)$ is the posterior probability defined as:

$$\gamma(t, l) = \frac{\alpha(M, l) \cdot \beta(M, l)}{p(\mathbf{Z}^V | \mathbf{Y}^V)}. \quad (23)$$

This result provides the foundation for optimizing the model using gradient descent.

D Analysis of FLOPs

Evaluating the computational complexity of LVLMs requires examining key components such as the self-attention mechanism and the feed-forward network (FFN). The total floating-point operations (FLOPs) can be expressed as $\text{FLOPs} = T \times (4nd^2 + 2n^2d + 2ndm)$, where T is the number of transformer layers, n is the sequence length, d is the hidden dimension size, and m represents the intermediate size of the FFN. During the training process, we can estimate $\mathbb{E}(n) \approx \frac{d}{4}$ and $m \approx 4d$, and this expression can be estimated as $\text{FLOPs} \approx T \times (12nd^2 + 2n^2d)$. This equation shows that computational complexity is strongly influenced by the sequence length n . In typical vision-language tasks, the sequence length is defined as $n = n_{\text{sys}} + n_{\text{img}} + n_{\text{ins}} + n_{\text{res}}$, with n_{img} often being much larger than the other three, sometimes by a factor of 20 [10, 21] as $n_{\text{img}} \approx 20 \times (n_{\text{sys}} + n_{\text{ins}} + n_{\text{res}})$. Thus, reducing n_{img} is essential for improving the efficiency of LVLMs. We analyze the expectations of FLOPs under two scenarios: (1) the original case where n is unchanged, and (2) the case where n is scaled by 1/8 by VCM with information domain $S = 1/4$. Let the variance of n be $\text{Var}(n) = \sigma_n^2$.

Original Expectation of FLOPs

The original expectation is:

$$\mathbb{E}_{\text{original}} = T \times (12d^2 \cdot \mathbb{E}(n) + 2d \cdot \mathbb{E}(n^2)). \quad (24)$$

Substituting $\mathbb{E}(n) = \frac{d}{4}$ and $\mathbb{E}(n^2) = \sigma_n^2 + \frac{d^2}{16}$, we get:

$$\mathbb{E}_{\text{original}} = T \times \left(\frac{25d^3}{8} + 2d \cdot \sigma_n^2 \right). \quad (25)$$

Scaled Expectation of FLOPs

When n is scaled by 1/8, the new expectation is:

$$\mathbb{E}_{\text{new}} = T \times (12d^2 \cdot \mathbb{E}(n') + 2d \cdot \mathbb{E}(n'^2)), \quad (26)$$

where $\mathbb{E}(n') = \frac{d}{32}$ and $\mathbb{E}(n'^2) = \frac{\sigma_n^2}{64} + \frac{d^2}{1024}$. Substituting these values gives:

$$\mathbb{E}_{\text{new}} = T \times \left(\frac{3d^3}{8} + \frac{d \cdot \sigma_n^2}{32} + \frac{d^3}{512} \right). \quad (27)$$

Ratio of Expectations of FLOPs

The ratio of the scaled expectation to the original expectation can be approximated by discarding negligible terms as follows:

$$R = \frac{\mathbb{E}_{\text{new}}}{\mathbb{E}_{\text{original}}} = \frac{\frac{3d^3}{8} + \frac{d \cdot \sigma_n^2}{32} + \frac{d^3}{512}}{\frac{25d^3}{8} + 2d \cdot \sigma_n^2} \approx \frac{\frac{3d^3}{8}}{\frac{25d^3}{8}} = \frac{3}{25}. \quad (28)$$

Therefore, the ratio approximately lies in the range $R \in [0, \frac{3}{25}]$. This shows that VCM can significantly reduce computational costs, for example, achieving an 85% reduction in FLOPs for LLaVA-1.5-7B.

E Additional Implementation Details

More details of evaluation. In addition to visual question answering and hallucination, we also use various benchmarks and datasets, such as zero-shot image classification, open-vocabulary object detection, and open-vocabulary semantic segmentation, to prove the visual concept enhancement capabilities. All these evaluation tasks and metrics are listed in table 9.

More Details of VCM. To further elaborate on the details of our method, we provide a comprehensive overview of the process described in section 4, along with the complete pseudocode for the training pipeline in algorithm 1. The VCM loss is derived through visual concept length estimation, objective expansion, forward and backward initialization, and state transitions. Gradients are then computed to enable end-to-end optimization.

More details of SM. To extract visual concepts from the most probable path, we employ the segment merging (SM) operation. However, since the length and number of visual concepts vary across samples, using a double for-loop for feature extraction introduces a significant computational bottleneck, severely reducing training efficiency. This limitation is one of the primary reasons previous methods [21, 9, 10, 8] avoid using variable-length features in end-to-end training.

To address this issue, we implement a parallelized SM operation capable of simultaneously handling multi-end features of varying lengths and positions. The PyTorch implementation of this operation is provided in algorithm 2. Compared to the double for-loop approach, our method achieves a 100x speedup, making the SM operation computationally efficient and effectively imperceptible during training.

F More Visualization Cases

To further demonstrate the effectiveness of our method, we provide additional visualization cases, including visual concept extraction in fig. 5, visual concept enhancement of the visual encoder in fig. 6, open-vocabulary object detection in fig. 8, and open-vocabulary semantic segmentation in fig. 7.

Table 9: **Overall descriptions of the evaluation benchmarks** for evaluating capabilities, visual question answering, comprehension, perception, and hallucination.

	Dataset	Task description	Eval Split	Metric
VQA.	VQAv2 [30]	Scene understanding QA	test-dev	VQA Acc (↑) [50]
	SciQA [29]	External knowledge QA	val	VQA Acc (↑) [50]
	GQA [25]	Scene understanding QA	test-dev	VQA Acc (↑) [50]
	VizWiz [51]	Scene understanding QA	test-dev	VQA Acc (↑) [50]
	MME [27]	External knowledge QA	val	VQA Acc (↑) [50]
PER.	ADE20K [35]	Open-Vocabulary Semantic Segmentation	val	mIoU, mAcc (↑) [52]
	COCO Panoptic [43]	Zero-shot Image Classify	val	Acc (↑)
	OV-COCO [46]	Open-Vocabulary Object Detection	val	$AP_{50}^{novel}, AP_{50}^{base}, AP_{50}, (\uparrow)$ [46]
Hall.	POPE-R [28]	Visual Hallucination	val	Acc (↑)
	POPE-P [28]	Visual Hallucination	val	Acc (↑)
	POPE-A [28]	Visual Hallucination	val	Acc (↑)
CPH.	MMBench [26]	Visual Comprehension	dev-en	Acc (↑)
	MMVet [32]	Visual Comprehension	val	Acc (↑)
	SEED [31]	Visual Comprehension	val	Acc (↑)

Figure 5: **More visualization of VCM on different instructions.** From left to right, the visual representation becomes increasingly sparse, leaving corresponding vision tokens to unmasked keywords (highlighted in red). VCM can capture the corresponding visual concepts relatively accurately by masking different numbers of keywords across different instructions, demonstrating the robustness and effectiveness of our approach.

Algorithm 1 Pseudocode of VCM Loss for Gradient Computation**Input:**

Probability sequence $\mathbf{Y}^V = [\mathbf{y}_1^V, \mathbf{y}_2^V, \dots, \mathbf{y}_M^V]$, where M is the input sequence length.
 Information domain scalar $S \in (0, 1/2]$, used for length adjustment.
 Mask ratio $r \sim \text{Uniform}(0, 1)$.

Output:

VCM loss \mathcal{L}_{VCM} and gradients $\frac{\partial \mathcal{L}_{\text{VCM}}}{\partial \mathbf{y}^V}$.

Initialization:

Define $L = \lfloor r \cdot M \cdot S \rfloor$: Length of the target sequence.
 Initialize target sequence \mathbf{x} with L symbols, randomly sampled as follows:

$$\mathbf{Z}^V = [\mathbf{z}_1^V, \mathbf{z}_1^V, \dots, \mathbf{z}_L^V], \quad \mathbf{z}_l^V \in \{\star\}.$$

Here, \star indicates retaining the current token, and \emptyset indicates discarding the current token.

Extend target sequence \mathbf{Z}^V by inserting \emptyset between and around symbols:

$$\mathbf{Z}^V = [\emptyset, \mathbf{z}_1^V, \emptyset, \mathbf{z}_2^V, \emptyset, \dots, \mathbf{z}_L^V, \emptyset].$$

The length of \mathbf{Z}^V is $2L + 1$.

Initialize forward variable $\alpha(M, l)$ and backward variable $\beta(M, l)$ to 0.
 Set $\alpha(1, 1) = \mathbf{y}_1^V(\emptyset)$ and $\beta(M, 2L + 1) = 1$.

Forward Pass:

for $t = 2$ **to** M **do**

for $l = 1$ **to** $2L + 1$ **do**

$$\alpha(M, l) = \mathbf{y}_t^V(\mathbf{z}_l^V) \cdot (\alpha(t - 1, l) + \alpha(t - 1, l - 1))$$

end for

end for

Backward Pass:

for $t = M - 1$ **to** 1 **do**

for $l = 2L$ **to** 1 **do**

$$\beta(M, l) = \beta(t + 1, l) \cdot \mathbf{y}_{t+1}^V(\mathbf{z}_l^V) + \beta(t + 1, l + 1) \cdot \mathbf{y}_{t+1}^V(\mathbf{z}_{l+1}^V)$$

end for

end for

Compute Loss:

$$p(\mathbf{Z}^V | \mathbf{Y}^V) = \sum_{l=1}^{2L+1} \alpha(M, l) \cdot \beta(M, l)$$

$$\mathcal{L}_{\text{VCM}} = -\log p(\mathbf{Z}^V | \mathbf{Y}^V)$$

Compute Gradients:

for $t = 1$ **to** M **do**

for $l = 1$ **to** $2L + 1$ **do**

 Compute posterior probability:

$$\gamma(t, l) = \frac{\alpha(M, l) \cdot \beta(M, l)}{p(\mathbf{Z}^V | \mathbf{Y}^V)}$$

 Compute gradient for $\mathbf{y}_t^V(\mathbf{z}_l^V)$:

$$\frac{\partial \mathcal{L}_{\text{VCM}}}{\partial \mathbf{y}_t^V(\mathbf{z}_l^V)} = \mathbf{y}_t^V(\mathbf{z}_l^V) - \gamma(t, l)$$

end for

end for

Optimization:

Update \mathbf{y}_t^V using gradient descent:

$$\mathbf{y}_t^V(\mathbf{z}_l^V) \leftarrow \mathbf{y}_t^V(\mathbf{z}_l^V) - \eta \cdot \frac{\partial \mathcal{L}_{\text{VCM}}}{\partial \mathbf{y}_t^V(\mathbf{z}_l^V)},$$

where η is the learning rate.

Algorithm 2 Pseudocode of Merging Segments with Scores (100x faster than a double loop)

```

def merge_segments_with_scores(x, x_mask, scores):
    """
    Merge adjacent features with mask=1 using score-weighted averaging,
    discarding features with mask=0.

    Args:
        x (torch.Tensor): Input features, shape [B, S, D].
        x_mask (torch.Tensor): Binary mask, shape [B, S].
        scores (torch.Tensor): Scores for each feature, shape [B, S].

    Returns:
        new_x (list[torch.Tensor]): Merged features, each element shape [N, D].
    """
    B, S, D = x.size()

    # Mask features and scores
    masked_x = x * x_mask.unsqueeze(-1)
    masked_scores = scores * x_mask

    # Extend mask and scores for cumulative sums
    expanded_x_mask = torch.cat([x_mask, torch.zeros((B, 1), dtype=x_mask.dtype,
                                                    device=x_mask.device)], dim=1)
    expanded_scores = torch.cat([scores, torch.zeros((B, 1), dtype=scores.dtype,
                                                    device=scores.device)], dim=1)

    # Compute cumulative sums
    cumsum_mask = torch.cumsum(expanded_x_mask, dim=1)
    cumsum_x = torch.cumsum(masked_x * scores.unsqueeze(-1), dim=1) # Weighted sum of features
    cumsum_scores = torch.cumsum(masked_scores, dim=1) # Cumulative sum of scores

    # Identify segment boundaries
    segment_mask = x_mask * ((cumsum_mask[:, 1:] - cumsum_mask[:, :-1]) == 0)
    new_x = []

    for i in range(B):
        # Extract cumulative sums and segment masks for the current sample
        cumsum_x_current = cumsum_x[i]
        cumsum_scores_current = cumsum_scores[i]
        cumsum_mask_current = cumsum_mask[i, :-1]
        segment_mask_current = segment_mask[i].bool()

        # Get segment-wise cumulative sums
        segment_sums = cumsum_x_current[segment_mask_current, :] # [N, D]
        segment_score_sums = cumsum_scores_current[segment_mask_current] # [N]

        # Extend cumulative sums for segment-wise computation
        expand_segment_sums = torch.cat([torch.zeros((1, D), dtype=segment_sums.dtype,
                                                    device=segment_sums.device), segment_sums])
        expand_segment_score_sums = torch.cat([torch.zeros((1, ), dtype=segment_score_sums.dtype,
                                                    device=segment_score_sums.device),
        segment_score_sums])

        diff_sums = expand_segment_sums[1:, :] - expand_segment_sums[:-1, :] # [N, D]
        diff_score_sums = expand_segment_score_sums[1:] - expand_segment_score_sums[:-1] # [N]

        # Prevent division by zero
        diff_score_sums = torch.where(diff_score_sums == 0, torch.ones_like(diff_score_sums),
        diff_score_sums)

        # Compute score-weighted mean
        weighted_mean_segments = diff_sums / diff_score_sums.unsqueeze(-1) # [N, D]

        new_x.append(weighted_mean_segments)

    return new_x

```

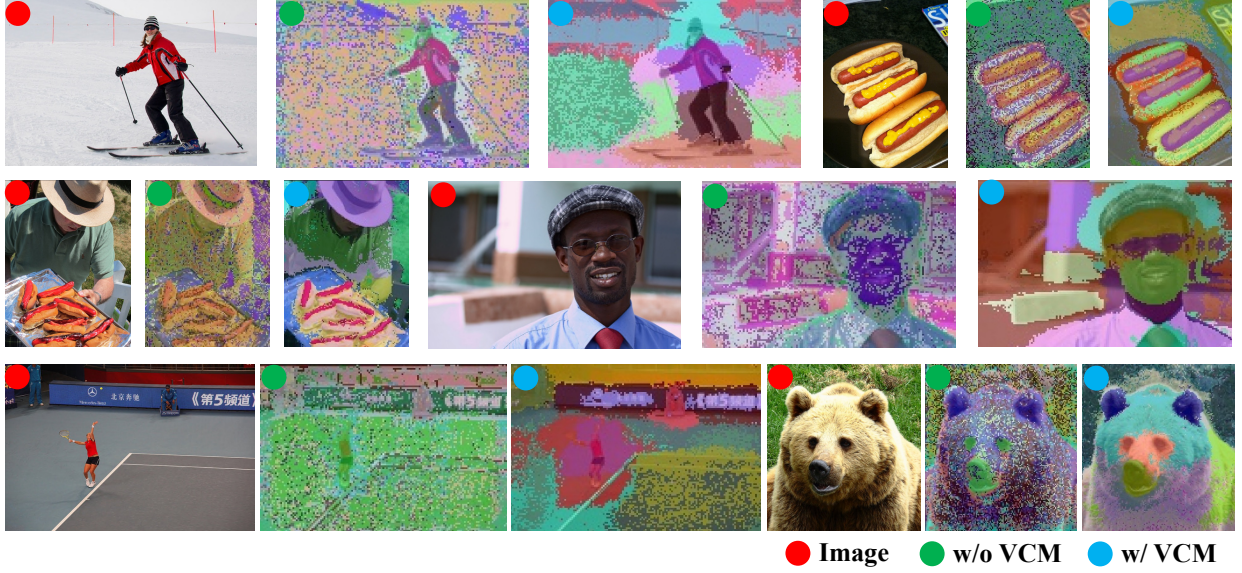


Figure 6: **More K-Means visualization of the dense feature maps of CLIP ViT trained in VCM.** We show the raw images, the K-Means results without VCM, and those of our fine-tuned model by VCM. As we can see, VCM has significant conceptual enhancements in multiple scenarios, such as animals, food, humans, and near and far perspectives, proving the generalizability and potential of our methods.



Figure 7: **Visualization of image segmentation.** The images are sampled from COCO val [34].

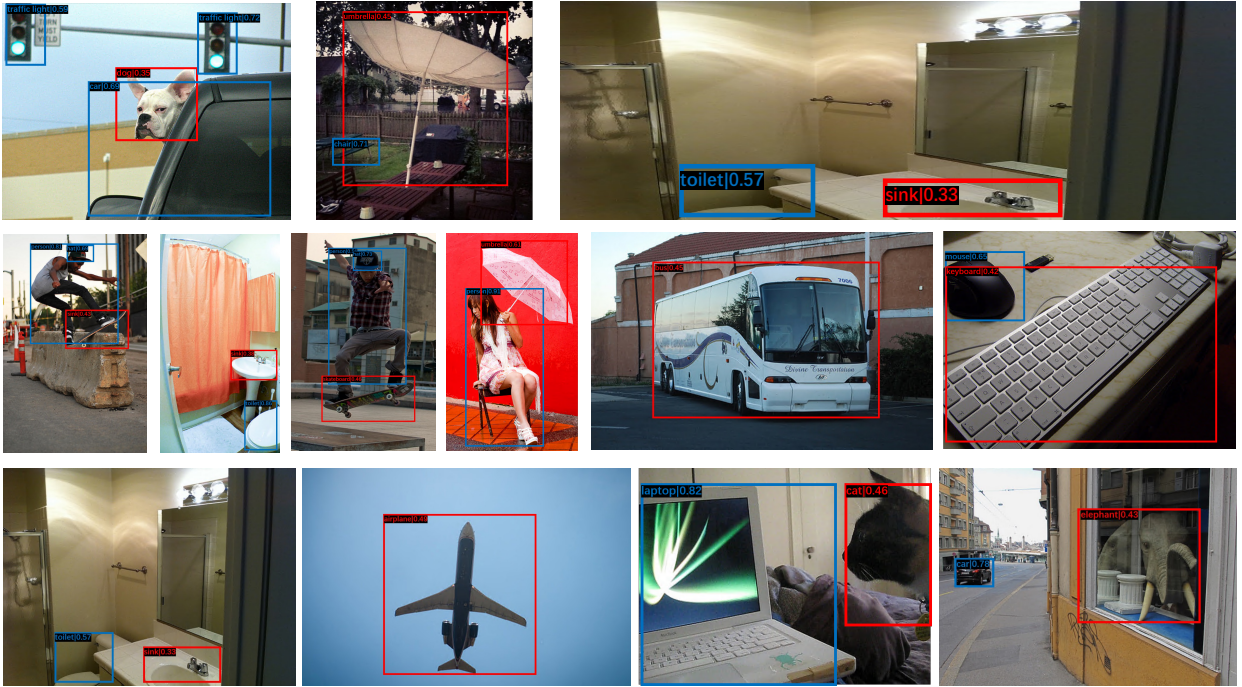


Figure 8: **Visualization of object detection results.** The red boxes are for the novel categories and the blue boxes are for the base categories.

References

- [1] Haotian Liu, Chunyuan Li, Qingyang Wu, and Yong Jae Lee. Visual instruction tuning. In *NeurIPS*, 2024.
- [2] Haotian Liu, Chunyuan Li, Yuheng Li, Bo Li, Yuanhan Zhang, Sheng Shen, and Yong Jae Lee. Llava-next: Improved reasoning, ocr, and world knowledge, January 2024.
- [3] Jinze Bai, Shuai Bai, Shusheng Yang, Shijie Wang, Sinan Tan, Peng Wang, Junyang Lin, Chang Zhou, and Jingren Zhou. Qwen-vl: A frontier large vision-language model with versatile abilities. *arXiv preprint arXiv:2308.12966*, 2023.
- [4] Wenliang Dai, Junnan Li, Dongxu Li, Anthony Meng Huat Tiong, Junqi Zhao, Weisheng Wang, Boyang Li, Pascale N Fung, and Steven Hoi. Instructblip: Towards general-purpose vision-language models with instruction tuning. In *NeurIPS*, 2024.
- [5] Run Luo, Yunshui Li, Longze Chen, Wanwei He, Ting-En Lin, Ziqiang Liu, Lei Zhang, Zikai Song, Xiaobo Xia, Tongliang Liu, et al. Deem: Diffusion models serve as the eyes of large language models for image perception. *arXiv preprint arXiv:2405.15232*, 2024.
- [6] Xiaobo Xia and Run Luo. Gui-r1: A generalist r1-style vision-language action model for gui agents. *arXiv preprint arXiv:2504.10458*, 2025.
- [7] Yiwei Zhou, Xiaobo Xia, Zhiwei Lin, Bo Han, and Tongliang Liu. Few-shot adversarial prompt learning on vision-language models. In *NeurIPS*, pages 3122–3156, 2024.
- [8] Wenbo Hu, Zi-Yi Dou, Liunian Harold Li, Amita Kamath, Nanyun Peng, and Kai-Wei Chang. Matryoshka query transformer for large vision-language models. *arXiv preprint arXiv:2405.19315*, 2024.
- [9] Yuan Zhang, Chun-Kai Fan, Junpeng Ma, Wenzhao Zheng, Tao Huang, Kuan Cheng, Denis Gudovskiy, Tomoyuki Okuno, Yohei Nakata, Kurt Keutzer, et al. Sparsevlm: Visual token sparsification for efficient vision-language model inference. *arXiv preprint arXiv:2410.04417*, 2024.
- [10] Senqiao Yang, Yukang Chen, Zhuotao Tian, Chengyao Wang, Jingyao Li, Bei Yu, and Jiaya Jia. Visionzip: Longer is better but not necessary in vision language models. *arXiv preprint arXiv:2412.04467*, 2024.
- [11] Lawrence R Rabiner. A tutorial on hidden markov models and selected applications in speech recognition. *Proceedings of the IEEE*, 77(2):257–286, 1989.
- [12] Run Luo, Haonan Zhang, Longze Chen, Ting-En Lin, Xiong Liu, Yuchuan Wu, Min Yang, Minzheng Wang, Pengpeng Zeng, Lianli Gao, et al. Mmevol: Empowering multimodal large language models with evol-instruct. *arXiv preprint arXiv:2409.05840*, 2024.
- [13] Run Luo, Lu Wang, Wanwei He, and Xiaobo Xia. Gui-r1: A generalist r1-style vision-language action model for gui agents. *arXiv preprint arXiv:2504.10458*, 2025.
- [14] Deyao Zhu, Jun Chen, Xiaoqian Shen, Xiang Li, and Mohamed Elhoseiny. Minigpt-4: Enhancing vision-language understanding with advanced large language models. *arXiv preprint arXiv:2304.10592*, 2023.
- [15] Runpei Dong, Chunrui Han, Yuang Peng, Zekun Qi, Zheng Ge, Jinrong Yang, Liang Zhao, Jianjian Sun, Hongyu Zhou, Haoran Wei, et al. Dreamllm: Synergistic multimodal comprehension and creation. *arXiv preprint arXiv:2309.11499*, 2023.
- [16] Run Luo, Ting-En Lin, Haonan Zhang, Yuchuan Wu, Xiong Liu, Min Yang, Yongbin Li, Longze Chen, Jiaming Li, Lei Zhang, et al. Openomni: Large language models pivot zero-shot omnimodal alignment across language with real-time self-aware emotional speech synthesis. *arXiv preprint arXiv:2501.04561*, 2025.
- [17] Youwei Liang, Chongjian Ge, Zhan Tong, Yibing Song, Jue Wang, and Pengtao Xie. Not all patches are what you need: Expediting vision transformers via token reorganizations. *arXiv preprint arXiv:2202.07800*, 2022.
- [18] Daniel Bolya, Cheng-Yang Fu, Xiaoliang Dai, Peizhao Zhang, Christoph Feichtenhofer, and Judy Hoffman. Token merging: Your vit but faster. *arXiv preprint arXiv:2210.09461*, 2022.
- [19] Jieneng Chen, Luoxin Ye, Ju He, Zhao-Yang Wang, Daniel Khashabi, and Alan Yuille. Efficient large multi-modal models via visual context compression. In *NeurIPS*, 2024.
- [20] Wenbo Hu, Zi-Yi Dou, Liunian Harold Li, Amita Kamath, Nanyun Peng, and Kai-Wei Chang. Matryoshka query transformer for large vision-language models. *arXiv preprint arXiv:2405.19315*, 2024.
- [21] Liang Chen, Haozhe Zhao, Tianyu Liu, Shuai Bai, Junyang Lin, Chang Zhou, and Baobao Chang. An image is worth 1/2 tokens after layer 2: Plug-and-play inference acceleration for large vision-language models. In *ECCV*, pages 19–35, 2025.

- [22] Long Xing, Qidong Huang, Xiaoyi Dong, Jiajie Lu, Pan Zhang, Yuhang Zang, Yuhang Cao, Conghui He, Jiaqi Wang, Feng Wu, et al. Pyramiddrop: Accelerating your large vision-language models via pyramid visual redundancy reduction. *arXiv preprint arXiv:2410.17247*, 2024.
- [23] Shaolei Zhang, Qingkai Fang, Zhe Yang, and Yang Feng. Llava-mini: Efficient image and video large multimodal models with one vision token. *arXiv preprint arXiv:2501.03895*, 2025.
- [24] Alec Radford, Jong Wook Kim, Chris Hallacy, Aditya Ramesh, Gabriel Goh, Sandhini Agarwal, Girish Sastry, Amanda Askell, Pamela Mishkin, Jack Clark, et al. Learning transferable visual models from natural language supervision. In *ICML*, pages 8748–8763, 2021.
- [25] Drew A Hudson and Christopher D Manning. Gqa: A new dataset for real-world visual reasoning and compositional question answering. In *CVPR*, pages 6700–6709, 2019.
- [26] Yuan Liu, Haodong Duan, Yuanhan Zhang, Bo Li, Songyang Zhang, Wangbo Zhao, Yike Yuan, Jiaqi Wang, Conghui He, Ziwei Liu, et al. Mmbench: Is your multi-modal model an all-around player? *arXiv preprint arXiv:2307.06281*, 2023.
- [27] Chaoyou Fu, Peixian Chen, Yunhang Shen, Yulei Qin, Mengdan Zhang, Xu Lin, Jinrui Yang, Xiawu Zheng, Ke Li, Xing Sun, et al. Mme: A comprehensive evaluation benchmark for multimodal large language models. *arXiv preprint arXiv:2306.13394*, 2023.
- [28] Yifan Li, Yifan Du, Kun Zhou, Jinpeng Wang, Wayne Xin Zhao, and Ji-Rong Wen. Evaluating object hallucination in large vision-language models. *arXiv preprint arXiv:2305.10355*, 2023.
- [29] Pan Lu, Swaroop Mishra, Tony Xia, Liang Qiu, Kai-Wei Chang, Song-Chun Zhu, Oyvind Tafjord, Peter Clark, and Ashwin Kalyan. Learn to explain: Multimodal reasoning via thought chains for science question answering. In *NeurIPS*, 2022.
- [30] Yash Goyal, Tejas Khot, Douglas Summers-Stay, Dhruv Batra, and Devi Parikh. Making the v in vqa matter: Elevating the role of image understanding in visual question answering. In *CVPR*, pages 6904–6913, 2017.
- [31] Bohao Li, Rui Wang, Guangzhi Wang, Yuying Ge, Yixiao Ge, and Ying Shan. Seed-bench: Benchmarking multimodal llms with generative comprehension. *arXiv preprint arXiv:2307.16125*, 2023.
- [32] Weihao Yu, Zhengyuan Yang, Linjie Li, Jianfeng Wang, Kevin Lin, Zicheng Liu, Xinchao Wang, and Lijuan Wang. Mm-vet: Evaluating large multimodal models for integrated capabilities. *arXiv preprint arXiv:2308.02490*, 2023.
- [33] Kaichen Zhang, Bo Li, Peiyuan Zhang, Fanyi Pu, Joshua Adrian Cahyono, Kairui Hu, Shuai Liu, Yuanhan Zhang, Jingkang Yang, Chunyuan Li, and Ziwei Liu. Lmms-eval: Reality check on the evaluation of large multimodal models, 2024.
- [34] Xinlei Chen, Hao Fang, Tsung-Yi Lin, Ramakrishna Vedantam, Saurabh Gupta, Piotr Dollár, and C Lawrence Zitnick. Microsoft coco captions: Data collection and evaluation server. *arXiv preprint arXiv:1504.00325*, 2015.
- [35] Bolei Zhou, Hang Zhao, Xavier Puig, Sanja Fidler, Adela Barriuso, and Antonio Torralba. Scene parsing through ade20k dataset. In *CVPR*, 2017.
- [36] Junnan Li, Dongxu Li, Silvio Savarese, and Steven Hoi. Blip-2: Bootstrapping language-image pre-training with frozen image encoders and large language models. In *ICML*, pages 19730–19742, 2023.
- [37] IDEFICS. Introducing idefics: An open reproduction of state-of-the-art visual language model. <https://huggingface.co/blog/idefics>, 2023.
- [38] Ziyi Lin, Chris Liu, Renrui Zhang, Peng Gao, Longtian Qiu, Han Xiao, Han Qiu, Chen Lin, Wenqi Shao, Keqin Chen, et al. Sphinx: The joint mixing of weights, tasks, and visual embeddings for multi-modal large language models. *arXiv preprint arXiv:2311.07575*, 2023.
- [39] Jiabo Ye, Anwen Hu, Haiyang Xu, Qinghao Ye, Ming Yan, Yuhao Dan, Chenlin Zhao, Guohai Xu, Chenliang Li, Junfeng Tian, et al. mplug-docowl: Modularized multimodal large language model for document understanding. *arXiv preprint arXiv:2307.02499*, 2023.
- [40] Yuzhang Shang, Mu Cai, Bingxin Xu, Yong Jae Lee, and Yan Yan. Llava-prumerge: Adaptive token reduction for efficient large multimodal models. *arXiv preprint arXiv:2403.15388*, 2024.
- [41] I Loshchilov. Decoupled weight decay regularization. *arXiv preprint arXiv:1711.05101*, 2017.
- [42] Stuart Lloyd. Least squares quantization in pcm. *IEEE Transactions on Information Theory*, 28(2):129–137, 1982.
- [43] Alexander Kirillov, Kaiming He, Ross Girshick, Carsten Rother, and Piotr Dollár. Panoptic segmentation. In *CVPR*, pages 9404–9413, 2019.

- [44] Kaiming He, Georgia Gkioxari, Piotr Dollár, and Ross Girshick. Mask r-cnn. In *ICCV*, pages 2961–2969, 2017.
- [45] Weicheng Kuo, Yin Cui, Xiuye Gu, AJ Piergiovanni, and Anelia Angelova. F-vlm: Open-vocabulary object detection upon frozen vision and language models. *arXiv preprint arXiv:2209.15639*, 2022.
- [46] Yuhang Zang, Wei Li, Kaiyang Zhou, Chen Huang, and Chen Change Loy. Open-vocabulary detr with conditional matching. In *ECCV*, pages 106–122, 2022.
- [47] Mengde Xu, Zheng Zhang, Fangyun Wei, Han Hu, and Xiang Bai. Side adapter network for open-vocabulary semantic segmentation. In *CVPR*, pages 2945–2954, 2023.
- [48] Holger Caesar, Jasper Uijlings, and Vittorio Ferrari. Coco-stuff: Thing and stuff classes in context. In *CVPR*, pages 1209–1218, 2018.
- [49] Seokju Cho, Heeseong Shin, Sunghwan Hong, Anurag Arnab, Paul Hongsuck Seo, and Seungryong Kim. Cat-seg: Cost aggregation for open-vocabulary semantic segmentation. In *CVPR*, pages 4113–4123, 2024.
- [50] Stanislaw Antol, Aishwarya Agrawal, Jiasen Lu, Margaret Mitchell, Dhruv Batra, C Lawrence Zitnick, and Devi Parikh. Vqa: Visual question answering. In *ICCV*, pages 2425–2433, 2015.
- [51] Danna Gurari, Qing Li, Abigale J Stangl, Anhong Guo, Chi Lin, Kristen Grauman, Jiebo Luo, and Jeffrey P Bigham. Vizwiz grand challenge: Answering visual questions from blind people. In *CVPR*, pages 3608–3617, 2018.
- [52] Jonathan Long, Evan Shelhamer, and Trevor Darrell. Fully convolutional networks for semantic segmentation. In *CVPR*, pages 3431–3440, 2015.